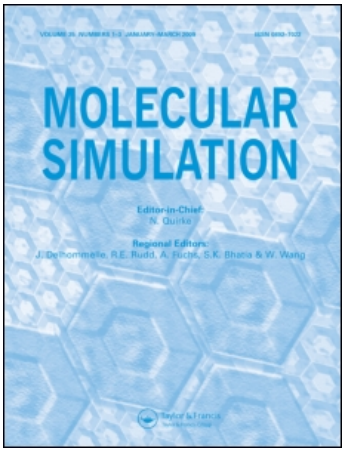

Molecular Simulation
Publication details, including instructions for authors and subscription information:
http://www.informaworld.com/smpp/title~content=t713644482

Molecular Dynamics Simulation of the Fast Ion Conductor δ-Bi_2O_3. III. Ionic Motion

D. A. Mac Dónaill[ab]; P. W. M. Jacobs[c]; Z. A. Rycerz[c]
[a] Department of Chemistry, Trinity College, Dublin 2, Republic of Ireland [b] Central Research Laboratory, Hitachi Ltd., Tokyo, Japan [c] Department of Chemistry, The University of Western Ontario, London, Ontario, Canada

To cite this Article Dónaill, D. A. Mac , Jacobs, P. W. M. and Rycerz, Z. A.(1990) 'Molecular Dynamics Simulation of the Fast Ion Conductor δ-Bi_2O_3. III. Ionic Motion', Molecular Simulation, 5: 3, 215 — 231
To link to this Article: DOI: 10.1080/08927029008022132
URL: http://dx.doi.org/10.1080/08927029008022132

Molecular Simulation, 1990, Vol. 5, pp. 215–231
Reprints available directly from the publisher
Photocopying permitted by license only

MOLECULAR DYNAMICS SIMULATION OF THE FAST ION CONDUCTOR δ-Bi_2O_3. III. IONIC MOTION

D.A. MAC DÓNAILL†

Department of Chemistry, Trinity College, Dublin 2, Republic of Ireland

P.W.M. JACOBS* and Z.A. RYCERZ*

Department of Chemistry, The University of Western Ontario, London, Canada N6A 5B7

(*Received October 1989, accepted December 1989*)

Dynamical aspects of molecular dynamics (MD) simulations are analysed with a view to determining the nature of fast-ion conduction in δ-Bi_2O_3. The ratio P_α of the moments of the self-correlation density distribution function, the velocity autocorrelation function (VAF), VAF integrals and VAF Fourier transforms, together with mean square displacement (MSD) data are interpreted in the light of experiment. It is shown that O^{2-} migration cannot adequately be described by either the hopping or liquid-like models of conduction but is best regarded as belonging to an intermediate category. Analysis of the fine structure of the P_α, MSD and VAF plots yields interesting correlations with vibrational modes.

KEY WORDS: Bismuth oxide, bismuth sesquioxide, fluorite, molecular dynamics, fast-ion conduction.

1. INTRODUCTION

In a previous paper [1] in this series [1,2] we examined the sub-lattice structure in δ-Bi_2O_3 in some detail. It was clear that the O^{2-} sub-lattice, far from having a simple, relatively featureless density distribution, was in fact highly structured, with significant interstitial density, the oxide ions being displaced from lattice sites along $\langle 100 \rangle$ and $\langle 111 \rangle$ directions. Small O^{2-} densities were also found in metastable positions half-way along cube-edges, through which migrating O^{2-} must pass. Structural details were found to be in excellent agreement with experimental results, thereby lending confidence to the model.

There is an extensive literature on Bi_2O_3, yet the true nature of the substance remains almost as elusive as ever. Many experimental reports are apparently mutually incompatible. Of particular note here is the ongoing controversy concerning the nature and extent of ordering within the O^{2-} sub-lattice. Classical works like that of Sillén [3] found a system with extensive $\langle 111 \rangle$ oxygen vacancy ordering. Others, e.g. [4,5], report a highly disordered system. Superstructures have also been reported [6]. Much of the confusion in the literature may have arisen because of the failure to recognise the existence of, not one, but two or more fcc fluorite forms, differing from each other in lattice constant and in the extent of order on the O^{2-} sub-lattice [7].

The fluorite phase of Bi_2O_3 is still far from being understood. The previous paper

† Currently at Central Research Laboratory, Hitachi Ltd., P.O. Box 2, Kokubunji, Tokyo 185, Japan.

* Associated with the Centre for Interdisciplinary Studies in Chemical Physics, The University of Western Ontario.

in this series [1] found Bi_2O_3 to have considerable structure, yet the entropy associated with the δ-phase is comparable with that of the liquid phase [8]. Accordingly, we focus our attention in this paper on the dynamic features of the system as elucidated by the molecular dynamics technique.

As in our previous papers we report here on four simulations. Two sets of potentials were used. The first, designated *R*, was based on electron-gas calculations whereas in the second, designated *D*, the Bi–O short-range potential was adjusted in order to reflect the high dielectric constant of the material while the retaining the rigid-on model. Calculations were also performed under two sets of conditions; firstly under experimental conditions (I), i.e. the conditions of temperature and density under which fast-ion conduction is observed and, secondly, under relaxed conditions, namely elevated temperatures and correspondingly expanded lattice constants. For the sake of completeness and convenience of reference these conditions are set out briefly in Table 1. Further details, may be found in [1,2]. Simulations under relaxed conditions proved necessary in order to overcome problems associated with approximations inherent in the model [2]. Fast-on conduction was only observed when the dielectrically adjusted potential set was employed under relaxed conditions (II-*D*2-2). In the other three simulations the system remains crystalline.

2. RESULTS AND DISCUSSION

2.1. P_α and Diffusion: Bi^{3+} Sub-Lattice

P_α is defined by

$$P_\alpha = \frac{3\langle[\Delta r(t)]_\alpha^4\rangle}{5\langle[\Delta r(t)]_\alpha^2\rangle^2} \tag{1}$$

where

$$\langle\Delta r(t)^{2n}\rangle = \frac{1}{N}\left\langle \sum_i^N [\mathbf{r}_i(0) - \mathbf{r}_i(t)]^{2n} \right\rangle = \int_0^\infty [\Delta \mathbf{r}(t)]^{2n} G_s(\mathbf{r},t)\, d\mathbf{r} \tag{2}$$

and

$$G_s(\mathbf{r},t) = \frac{1}{N}\left\langle \sum_i^N \delta[\mathbf{r} + \mathbf{r}_i(0) - \mathbf{r}_i(t)] \right\rangle \tag{3}$$

is the probability that, in the time-interval t, the displacement of a particular ion (of species α) lies within the volume element $d\mathbf{r}$ at $\mathbf{r}$. In the equations above, α denotes the kind of ions under consideration and $\langle\ \rangle$ brackets denote averaging over time origins. In fact $G_s(\mathbf{r},t)$ is identical with the Van Hove self-correlation function [9] for a classical system, in which the position vectors commute. For a Gaussian distribution of $G_s^\alpha(\mathbf{r},t)$ in $\mathbf{r}$, $P_\alpha = 1$. We should expect $P_\alpha = 1$ when each ion in the simultion is simply vibrating about its lattice site, and again when the motion is liquid-like [10,11]. Thus the calculation of P_α provides a simple means of determining whether the conduction mechanism is liquid-like or not [10].

P_α for the Bi^{3+} sub-lattice for all four simulations is depicted in Figure 1. In all four cases P_α is well behaved (i.e. = 1) from which we conclude that the Bi^{3+} sub-lattice is crystalline as the alternative interpretation would imply an isotropic liquid-like distribution for Bi^{3+}.

Table 1 Simulation conditions: I, II indicate *experimental* and *relaxed* conditions; *R*, *D* denote rigid-ion or dielectrically adjusted potential.

MD run	*Lattice Constant [Å]*	*Equilibrated Temperature [K]*	*Figure Reference*
I-*R*1	5.644	1017	a
I-*D*1	5.644	1026	b
II-*R*2-2	5.721	1489	c
II-*D*2-2	5.721	1489	d

Mean square displacement (MSD) plots confirm that no Bi^{3+} diffusion occurs (Figure 2). The strong vibrations in the MSD are most noticeable. From graphical analysis of Figure 2a (simulation I-*R*1) we estimate a frequency of 1.9 $\pm$ 0.5 THz. These vibrations are modulated by a second one which has an estimated frequency of 4.3 $\pm$ 0.6 THz. These frequencies indicate that the vibrations are those of the heavier Bi^{3+} atoms. In simulation I-*D*1 the period of vibration has increased slightly. Ex-

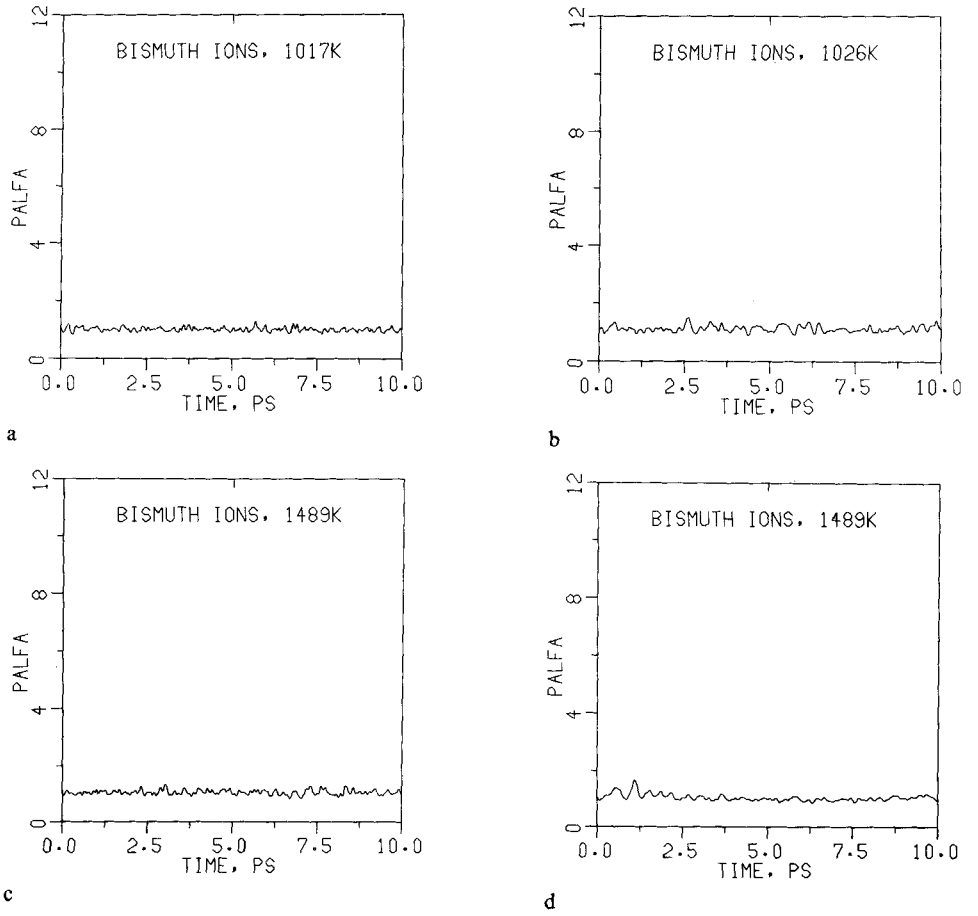

Figure 1 P_α for Bi^{3+}. The same designations (a) I-*R*1; (b) I-*D*1; (c) II-*R*2-2 and (d) II-*D*2-2 are followed in **all the figures** except 11. This designation is included in Table 1 as a ready reference.

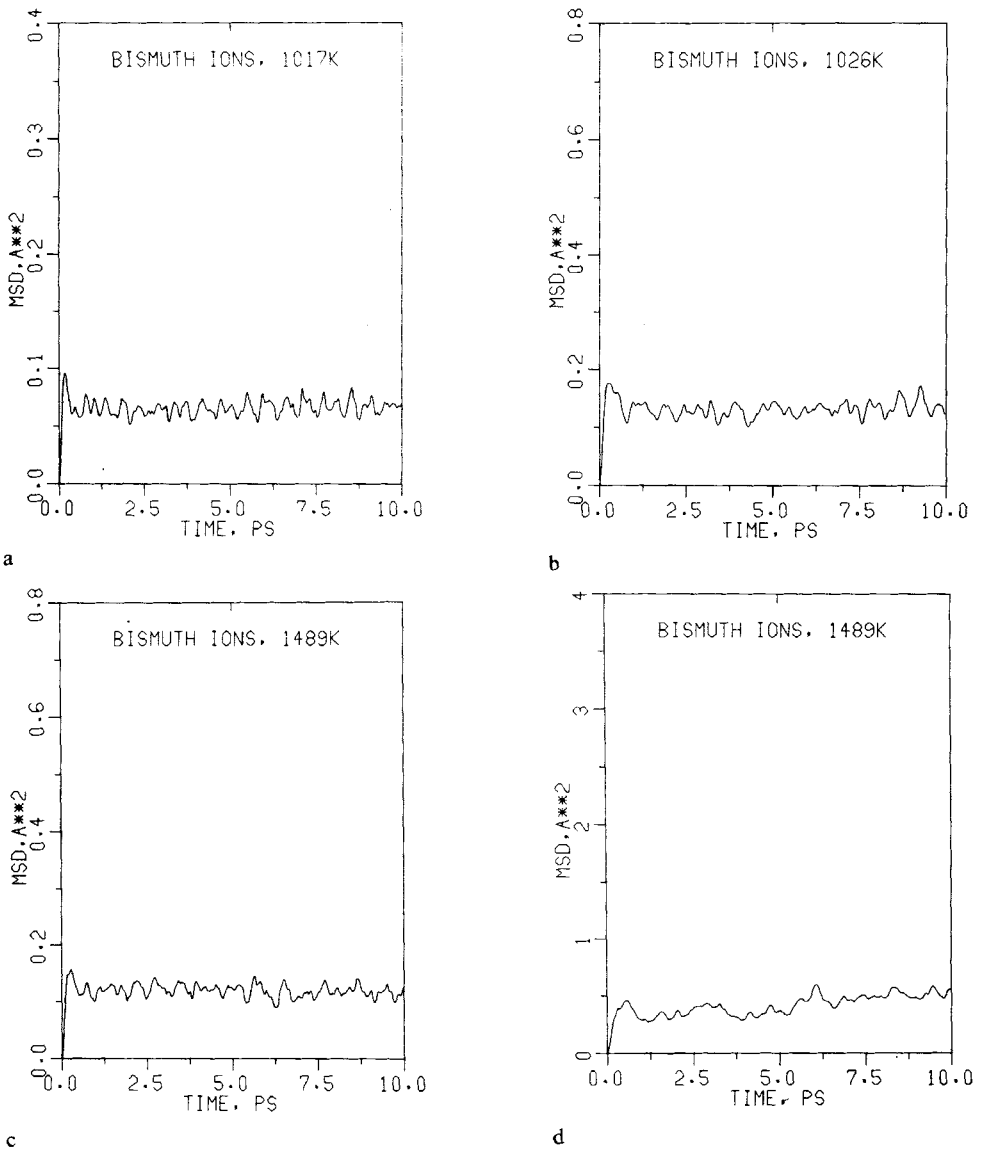

Figure 2 MSD for Bi^{3+}, (a) to (d) having the usual connotations.

Table 2 Experimental phonon energies from Pettsol'd [11].

$\hbar\omega_{ac}$ [meV]	$\hbar\omega_{opt}^{min}$ [meV]	$\hbar\omega_{opt}^{max}$ [meV]
8.2 ± 0.2	29.2 ± 0.8	30.5 ± 1.0
16.2 ± 0.5	57.3 ± 1.8	59.1 ± 1.6
66.6 ± 2.0	223.2 ± 6.6	229.4 ± 6.6

perimental data on the vibrational spectra of δ-Bi_2O_3 were unavailable to us. The α-phase, however, is a distorted fluorite phase and one might expect the crystalline δ-phase present in simulations I-*R*1, I-DI and II-*R*2-2, where no fast-ion conduction occurs, to bear a strong resemblance to it. Pettsol'd [12] has reported acoustic phonon energies for α-Bi_2O_3 of 2.00 ± 0.05 THz (8.2 ± 0.2 meV) and 3.92 ± 0.12 THz (16.2 ± 0.5 meV)-the agreement is clearly excellent. The vibration frequencies reported by Pettsol'd are summarized in Table 2.

The discernable vibrational period in the MSD plots for simulations I-*R*1, I-*D*1 and II-R2-2 reflects some degree of correlation. Independently vibrating Bi^{3+}'s would show a horizontal straight line in the MSD plot. In II-*D*2-2, however, the vibrating Bi^{3+}'s have a much greater vibrational amplitude, occasionally even penetrating the O^{2-} cage about them (Figure 16b in [1]). The vibrating Bi^{3+}'s will thus experience regions of the potential energy surface of considerable anharmonicity with force constants characteristic of other frequencies, thereby resulting in band broadening and loss of structure. Consequently the vibrational structure in the MSD of simulation II-*D*2-2 (Figure 2d) is much more poorly resolved. Moreover, the fast-ion conduction in the O^{2-} sub-lattice in this simulation is likely to weaken the correlation in the Bi^{3+} sub-lattice, also resulting in less structure in the MSD plots.

2.2. P_α and Diffusion: O^{2-} Sub-Lattice

$P_\alpha = 1$ in simulation I-*R*1 until 7 ps have elapsed (Figure 3a) after which large high-frequency vibrations may be observed. These vibrations are characteristic of isolated hops [10]. The region of large oscillations is characterised by two vibrations. The longer period is a little over 0.66 ps or 1.5 THz. This rather low frequency may have it origin in interactions with the Bi^{3+} sub-lattice and the reported 2 THz band (Table 2). Alternatively, it may represent the attempt frequency i.e., the frequency with which the O^{2-} ions attack the potential barrier of ~ 0.4 eV that limits their jumping to equivalent sites, or the frequency of the rather violent oscillations of an ion that has just made a successful jump, as it disposes of the excess kinetic energy carried with it during the jump. (These are probably the same modes). A second vibration of much higher frequency modulates the first. Graphical analysis yields an estimate of 15. $\pm$ 2. THz. This matches two bands reported by Pettsol'd, namely those at 13.9 ± 0.4 THz (57.3 ± 1.8 meV) and 14.3 ± 0.4 THz (59.1 ± 1.6 meV).

P_α for simulations I-*D*1 and II-*R*2-2 are essentially similar, being better behaved than I-*R*1. They nonetheless oscillate about $P_\alpha = 2$, which is not characteristic of a liquid, or a homogeneous distribution. P_α rises to approximately 4 in II-*R*2-2. In II-*R*2-2 P_α actually returns to 1 for a period of about 1.5 ps. Under both dielectrically adjusted and relaxed conditions in simulation II-*D*2-2 the noise in P_α is much lower.

The MSD plots for I-*R*1, I-*D*1 and II-*R*2-2 show no O^{2-} diffusion of significance. In I-*R*1 there is a characteristic period of 1.5 THz (see above) and this is modulated by a higher frequency oscillation. MSD plots are somewhat noisier in I-*D*2 and II-*R*2-2 but only in II-*D*2-2 is O^{2-} diffusion observed with a value of 0.24 [10^{-5} cm^2 s^{-1}] calculated from MSD. This value is comparable to diffusion in non-electrolytes, and strong and weak electrolytes in aqueous solutions (Table 3).

The large amplitude of the vibrational noise in I-*R*1 suggests that O^{2-} motion is strongly correlated. Both the O^{2-} and Bi^{3+} sub-lattices must relax in response to a change in environment, thus an O^{2-} hop indicates a period of greatly increased vibrational activity in the region of the hop, with frequencies characteristic of two sub-lattices.

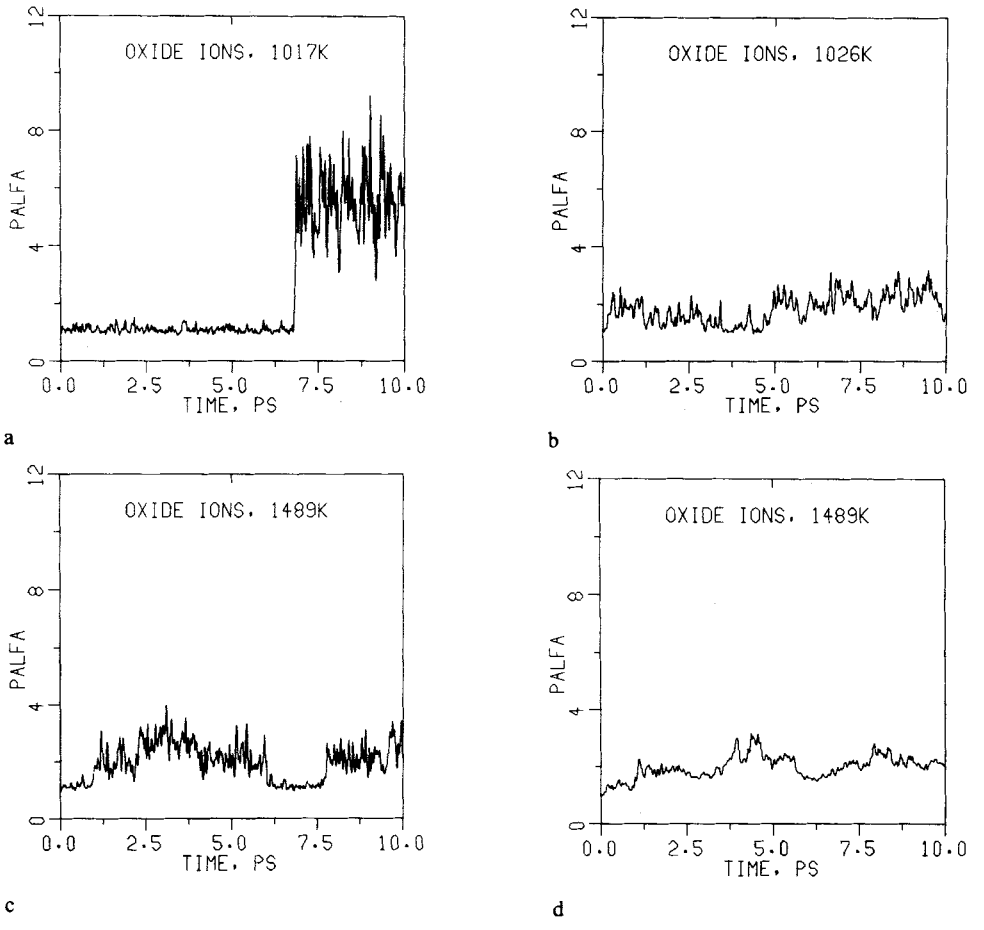

Figure 3 P_α for O^{2-}.

Simulations I-*D*1 and II-*R*2-2 exhibit a more uniform behaviour of Pα with deviations from unity observed over the whole time window. In I-*D*1 (Figure 3b) the characteristic frequency is approximately 6.1 THz. The fall in frequency by a factor of two is certainly due to broadening of potential wells due to dielectric adjustment of the potentials. II-*R*2-2 (Figure 3c) alternates between a crystalline state ($P_\alpha = 1$) and periods of large oscillations caused by isolated hops. In simulation II-*D*2-2 (Figure 3d), however, where fast-ion conduction is observed, the noise is greatly reduced. The value of P_α never strays far from 2 although considerable fluctuation remains. Thus P_α is characteristic of neither isotropic liquid-like behaviour nor isolated hops. δ-Bi_2O_3 is therefore best described as having a conduction mechanism intermediate in nature, between hopping and liquid-like, with O^{2-} jumps not continuous but nevertheless not isolated. MSD plots show that no diffusion occurs except in II-*D*2-2 where we observe fast-ion conduction. Calculated values for diffusion coefficients are listed in Table 3.

It should be noticed that a direct calculation of any correlation function in which all time or space origins are taken, requires cpu time proporitonal to the square of number of time steps or to N_α^2, where N_α is a number of particles of the kind under

Table 3a Diffusion coefficients of Bi^{3+} in δ-Bi_2O_3. The coefficients in first 5 columns are calculated from MSD for the last 200, 700 . . . 2 000 time steps of the simulation (standard deviations in brackets). In the last column are given diffusion coefficients calculated from VAF over 2 048 last steps. Units: [10^{-5} $cm^2 s^{-1}$].

MD run	D_{200}	D_{700}	D_{1000}	D_{1800}	D_{2000}	D_{VAF}
I-*R*1	0.0009	−0.0007	0.0006	0.0008	0.0006	0.1175
	(0.0016)	(0.0004)	(0.0002)	(0.0001)	(0.0001)	
I-*D*1	−0.0360	0.0044	0.0035	0.0022	0.0014	0.1245
	(0.0052)	(0.0008)	(0.0004)	(0.0002)	(0.0002)	
II-*R*2-2	0.0024	0.0003	−0.0009	−0.0017	−0.0009	0.1670
	(0.0034)	(0.0006)	(0.0004)	(0.0002)	(0.0002)	
II-*D*2-2	0.0698	0.0410	0.0390	0.0440	0.0401	0.2460
	(0.0132)	(0.0020)	(0.0017)	(0.0007)	(0.0007)	

Table 3b Diffusion coefficients of O^{2-} in δ-Bi_2O_3 Units: [10^{-5} $cm^2 s^{-1}$]; description as in the heading of Table 3a.

MD run	D_{200}	D_{700}	D_{1000}	D_{1800}	D_{2000}	D_{VAF}
I-*R*1	0.0102	0.0066	0.0153	0.0080	0.0068	1.40
	(0.0032)	(0.0007)	(0.0004)	(0.0002)	(0.0002)	
I-*D*1	−0.0526	0.0138	0.0036	0.0230	0.0159	1.43
	(0.0074)	(0.0014)	(0.0010)	(0.0006)	(0.0006)	
II-*R*2-2	0.0708	0.0212	0.0058	−0.0062	−0.0017	2.07
	(0.0059)	(0.0012)	(0.0009)	(0.0004)	(0.0004)	
II-*D*2-2	0.544	0.0983	0.145	0.292	0.318	2.41
	(0.0262)	(0.0063)	(0.0053)	(0.0027)	(0.0024)	

consideration. Therefore, these calculations are always expensive and they usually require much more cpu time than the MD simulation itself. For this reason the diffusion coefficients calculated, by a linear regression, from MSD (D_{MSD}) have been calculated for a single time origin and in each case averaged over all available particles (i.e. N_α). These D_{MSD} are presented in Tables 3a and 3b together with the coefficients calculated by FFT of VAF (D_{VAF}). The latter have been averaged over all possible time origins (in this case 2048).

2.3.a. Velocity Autocorrelation Function: Bi^{3+} Sub-lattice

The Bi^{3+} Velocity Autocorrelation Functions (VAF's) for all four simulations are shown in figure 5. In simulation I-R1 (Figure 5a) we observe a period of approximately 4.5 THz (18.6 meV), presumably reflecting the same phenomenon as the 4.3 THz observed in the MSD plot. The VAF is structured, damping is slow and the period increases with time. In I-*D*1 (Figure 5b) a period of 3.3 THz is found (13.6 meV). The fall in frequency is probably due to a broadening of the potential wells by the adjusted short-range potentials. Much of the structure in the VAF is gone, and damping is quite rapid. The first minimum is shallower than in I-R1 and this also is caused by damping. Simulations II-*R*2-2 (Figure 5c) and II-*D*2-2 (Figure 5d) echo simulations I-*R*1 and I-*D*1, with observed frequencies of 4.1 THz (17.0 meV) and 3.3 THz (13.6 meV) respectively. In II-D2-2 (Figure 5d) the first well is the shallowest of all four simulations.

The VAF integrals are displayed in Figure 6 and VAF Fast Fourier Transforms in

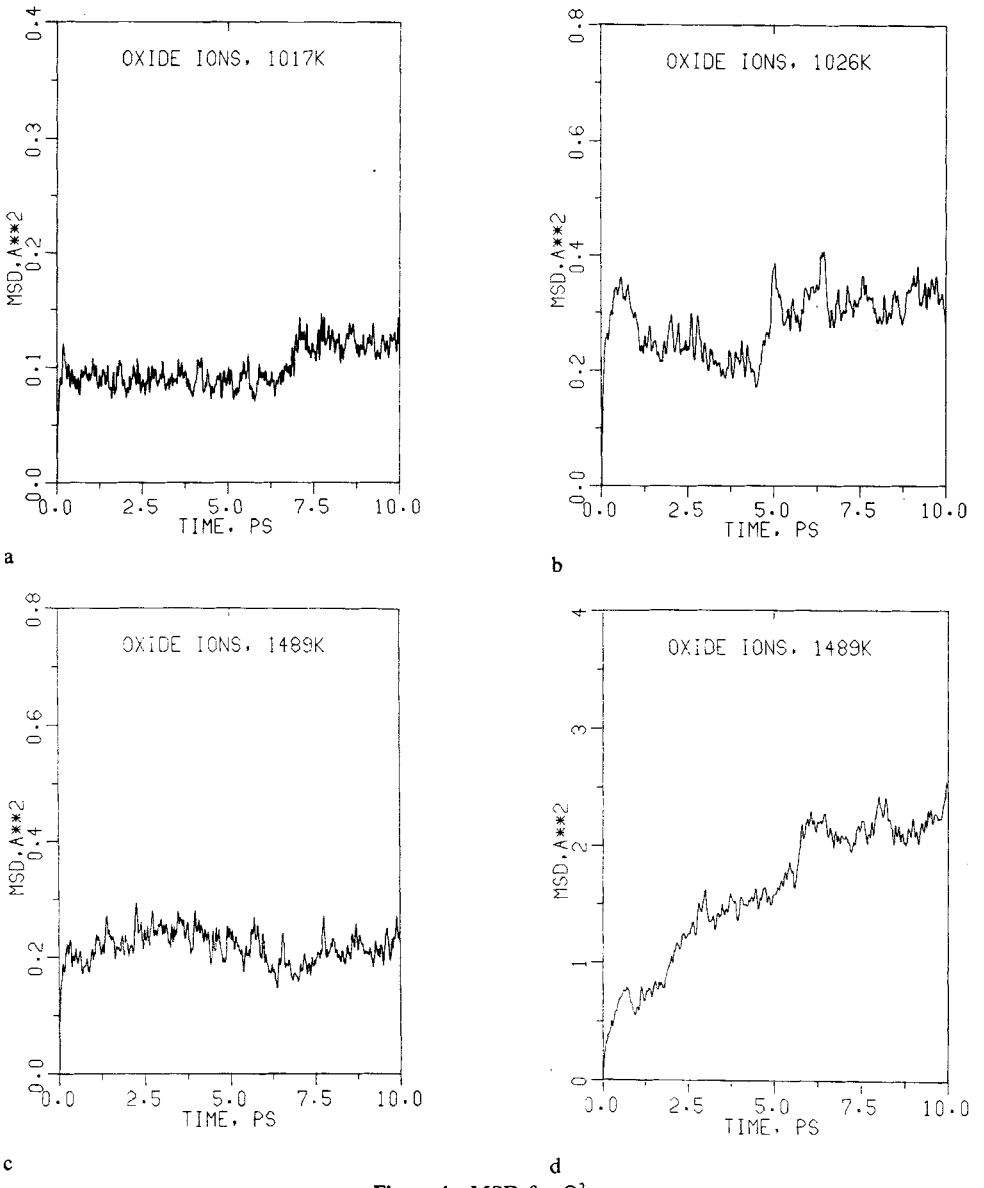

Figure 4 MSD for O^{2-}.

Figure 7. In the FT of the VAF for I-*R*1 there is a band stretching from 1.5–6.25 THz with a maximum at 3.75 THz close to the 4.0 THz observed in the MSD plots. In I-*D*1 the frequency distribution is shifted as a whole to the left, i.e. to lower frequencies, with a maximum at 2 Thz, close to the experimentally observed 8 meV. On II-*R*2-2 the bands once again drift to higher frequencies and back to lower frequencies again with II-*D*2-2. For the dielectrically adjusted potentials there is a maximum at approximately 2 THz with a shoulder at 4 THZ, in excellent agreement with the observed acoustic

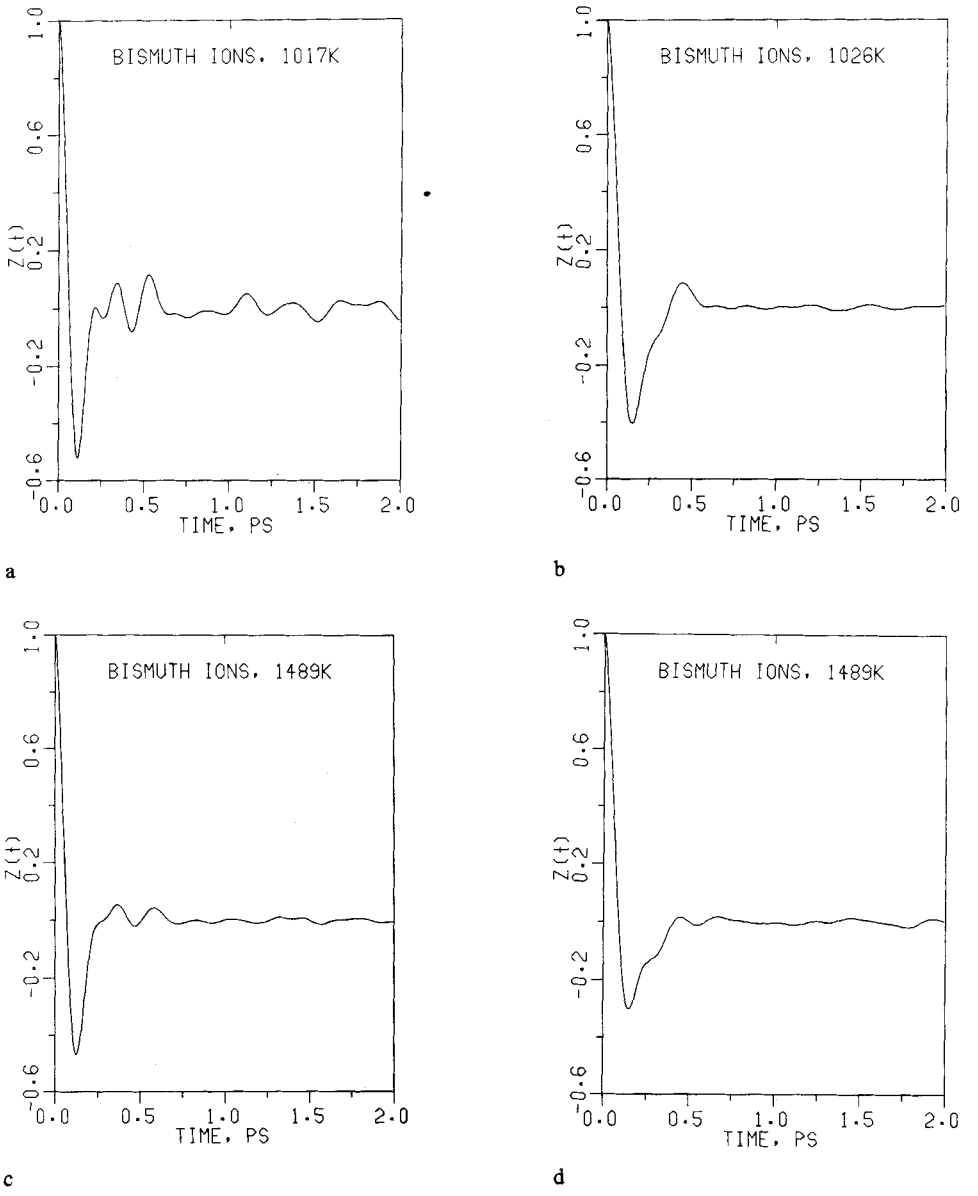

Figure 5 VAF for Bi^{3+}.

bands at 8.2 meV (1.98 THz) and 16.2 meV (3.91 THz). Thus the dielectrically adjusted potentials appear to yield a better description of the Bi^{3+} sub-lattice.

Calculated diffusion (D) values from the VAF integral and VAF FT are approximately 0.12 to 0.25 [10^{-5} cm^2 s^{-1}] which although small, disagrees with the values in the range -0.002 to 0.07 [10^{-5} cm^2 s^{-1}] obtained from MSD (i.e. essentailly zero). This suggests that the VAF may over-estimate D in crystalline systems.

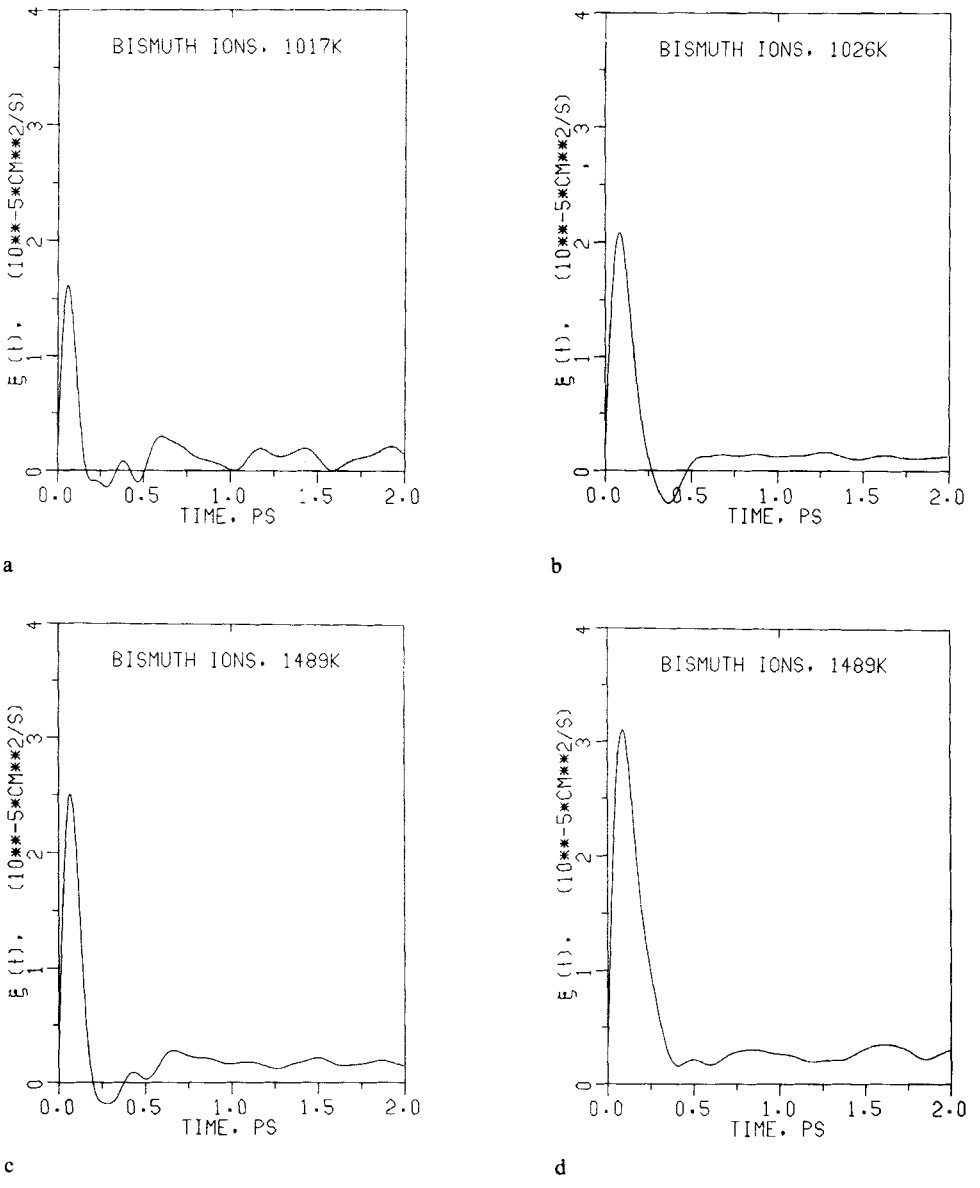

Figure 6 Integral of VAF for Bi^{3+}.

2.3.b Velocity Autocorrelation Function: O^{2-} Sub-lattice

In contrast to Bi^{3+} the VAF's for O^{2-} are considerably more structured. In I-*R*1 we observe a frequency of 17.3 THz (Figure 8a) falling to 14.6 THz in I-*D*1. Similar frequencies are observed in simulations II-*R*2-2 and II-*D*2-2. This 14.5–17.5 THz region lies between the main peaks in the VAF FT (Figure 9). These bands compare well with the acoustic 66.6 meV (16.1 THz) band and the optical 57.3–59.1 meV

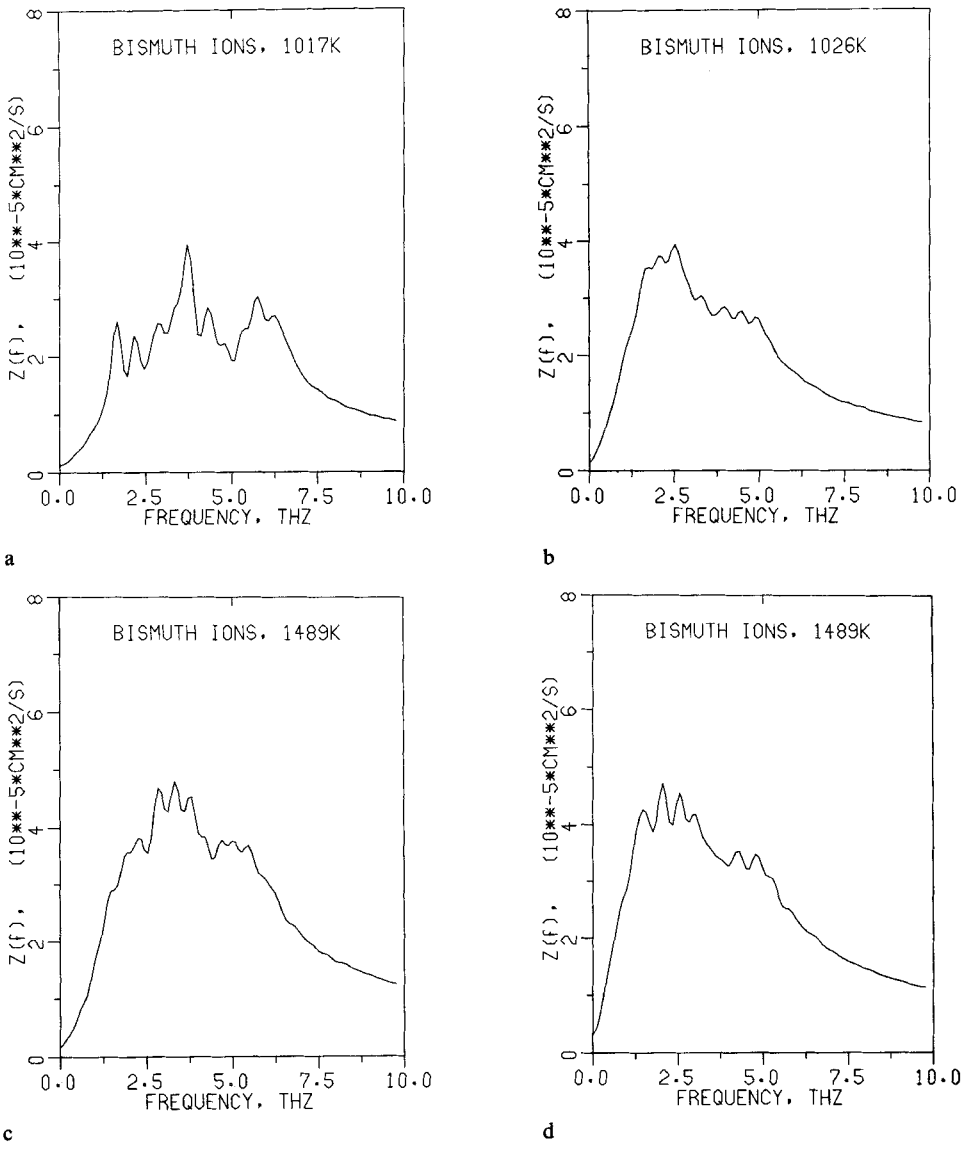

Figure 7 FFT of VAF for Bi^{3+}.

(13.9–14.3 THz) phonon bands [12]. As with Bi^{3+} the spectrum shows the expected shifts to lower frequencies on going from I-*R*1 to I-*D*1 and from II-*R*2-2 to II-*D*2-2.

The diffusion values for I-*R*1, I-*D*1 and II-*R*2-2 (Table 3) are clearly in error, being too large for systems which are obviously crystalline. The MSD values for these simulations, amounting to zero diffusion within experimental error are much more reasonable. High diffusion values were also calculated for Bi^{3+}. For example, the value of 2.41 [10^{-5} cm^2 s^{-1}] for simulation II-*D*2-2 is only marginally greater than that for II-*D*2-2 of 2.07 [10^{-5} cm^2 s^{-1}] where the system was crystalline. Thus the values for

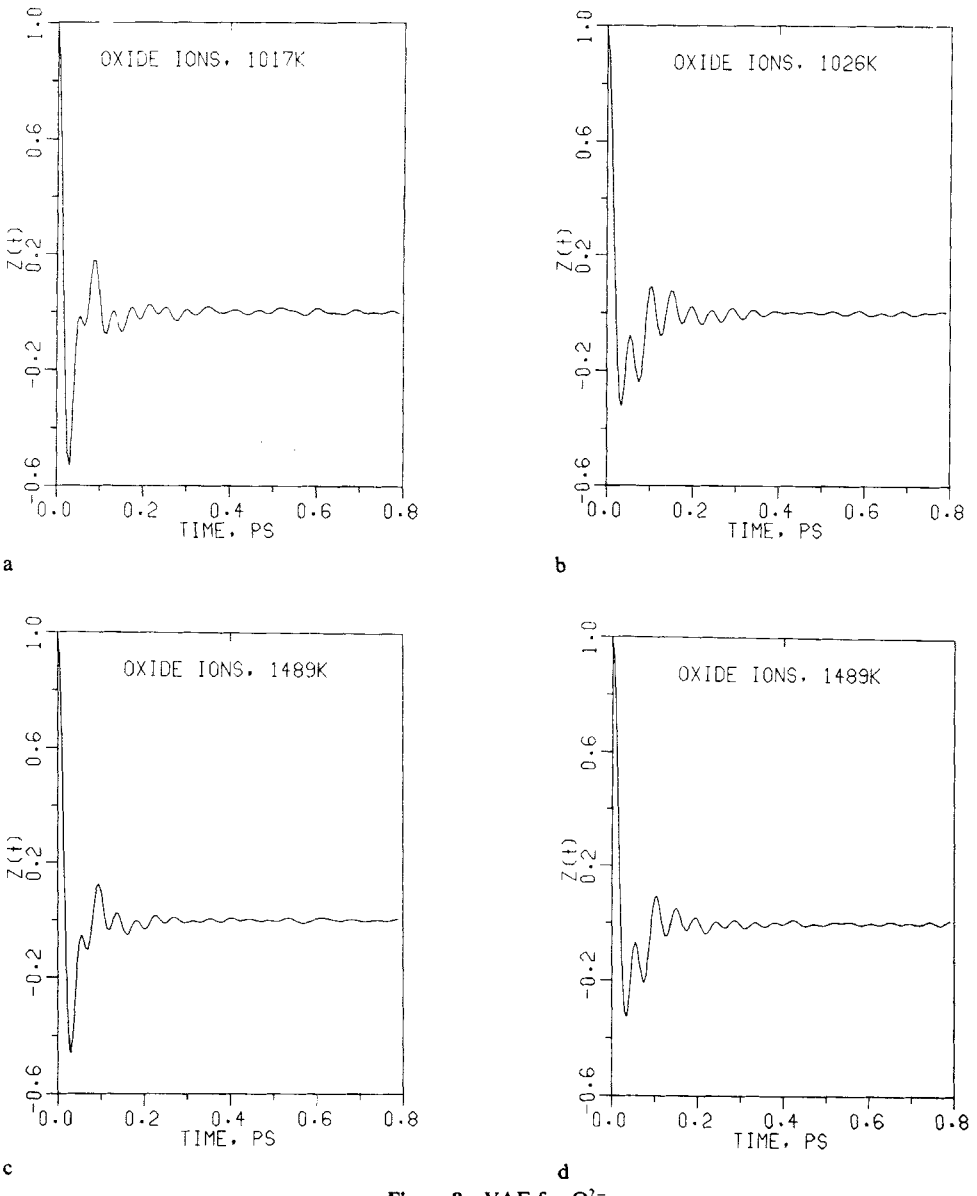

Figure 8 VAF for O^{2-}.

diffusion coefficients estimated from the FT of the VAF's appear unreliable for this system.

2.4. Migration Mechanisms

O^{2-} migrations are observed in all 4 simulations but only occur on a significant scale in II-*D*2-2. In all four simulations migrations occur along cube-edges (≪ 100 ≫

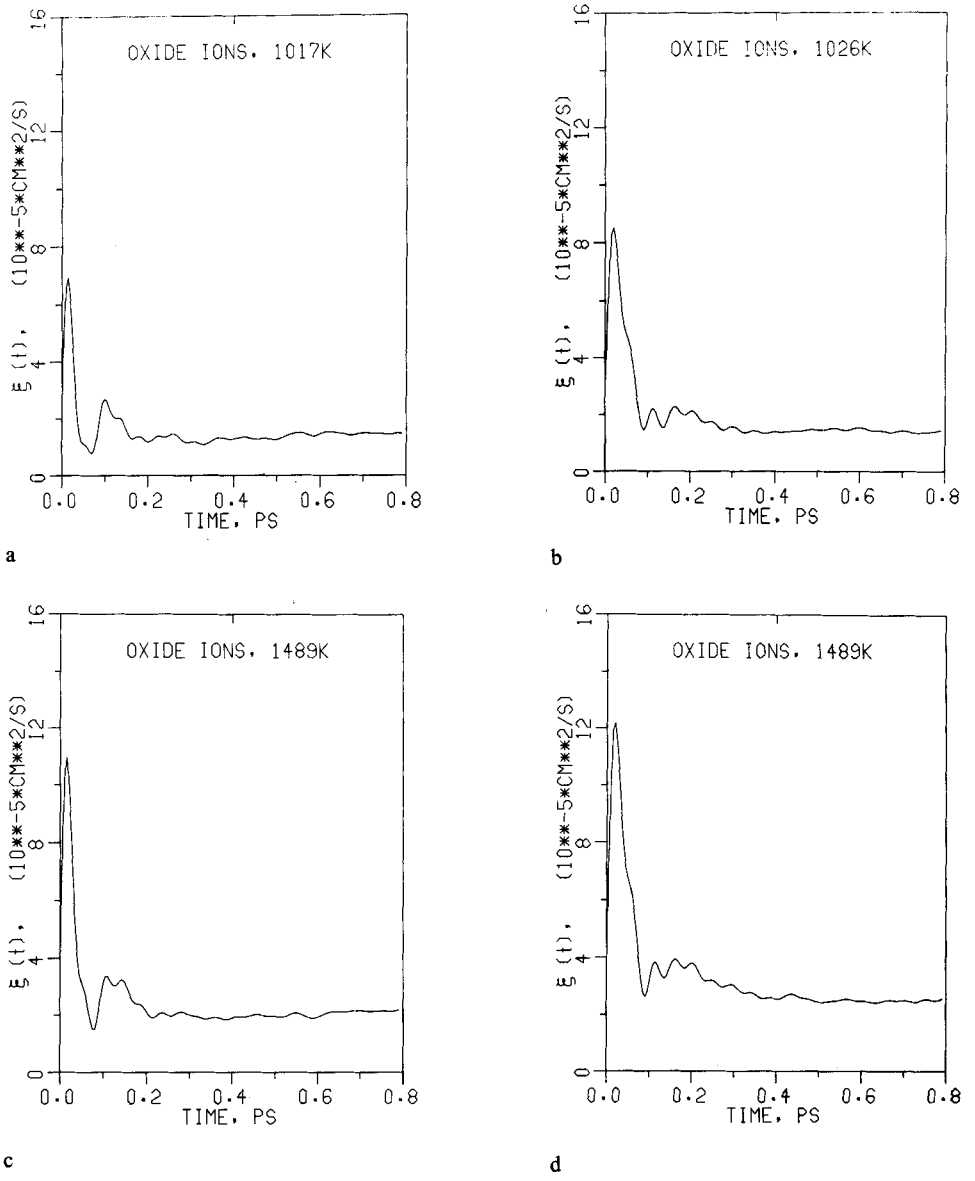

Figure 9 Integral of VAF for O^{2-}.

directions). Some jumps are direct but on other occasions the migrations occur via interstitial positions, half way along a cube-edge and displaced slightly towards a vacant cube-centre along a $\langle 110 \rangle$ direction. Both migration pathways may be observed clearly in the trajectory plots (Figure 11). The density of the interstitials at these site is such that they cannot be resolved on the density plots of the (100) or (110) planes (Figures 11 and 12 in [1]). However, they can be seen in the O^{2-} density in the Bi^{3+} (400) plane (Figure 16a in [1]).

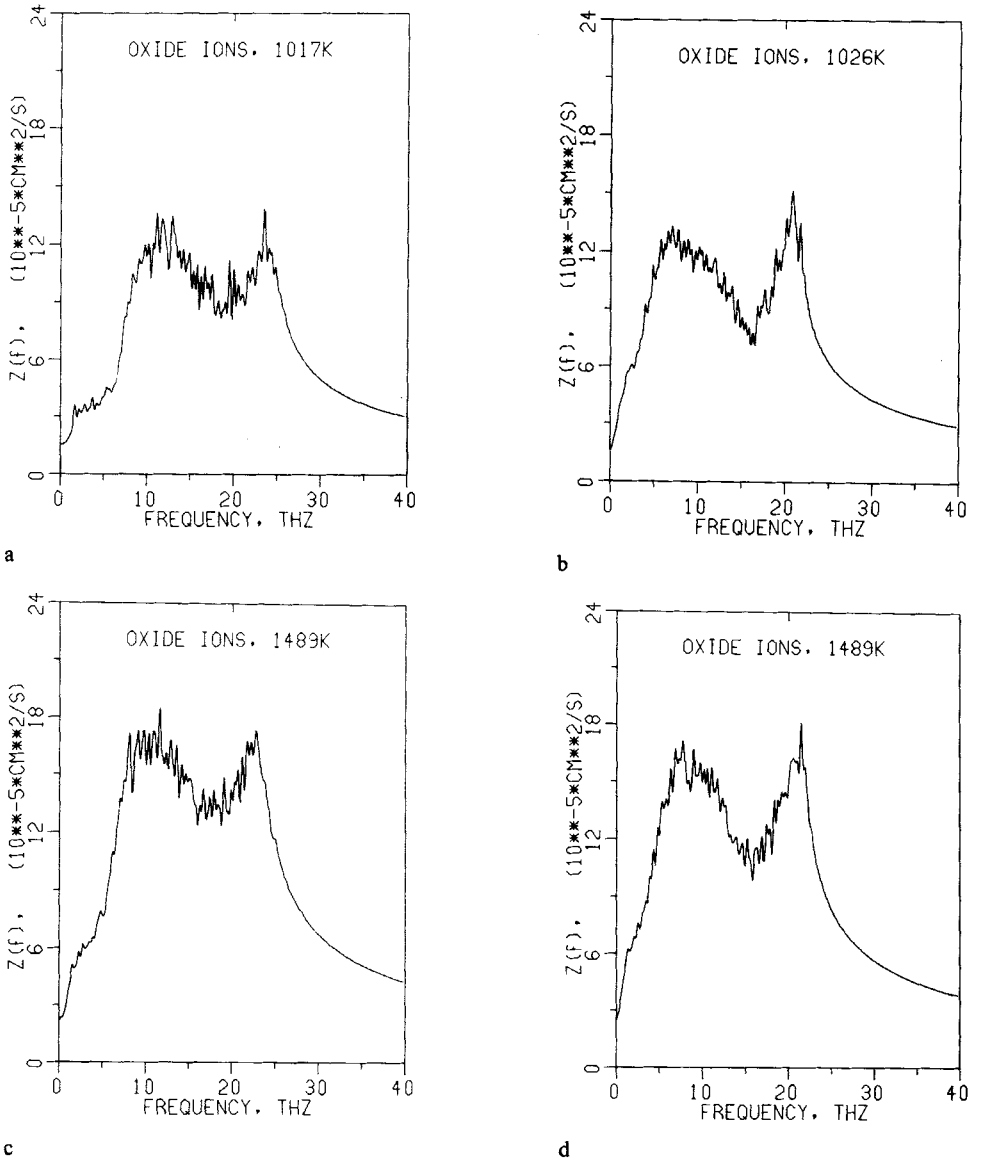

Figure 10 FFT of VAF for O^{2-}.

3. CONCLUSIONS

One of the greatest challenges faced in analysing these calculations was the paucity of detailed experimental information. Fortunately, some vibrational information on the closely related α-phase was available and this agrees well with the calculated vibrational frequencies deduced from the structure in the P_α, MSD and VAF plots.

Perhaps the most interesting result was that of P_α which indicated that the mechan-

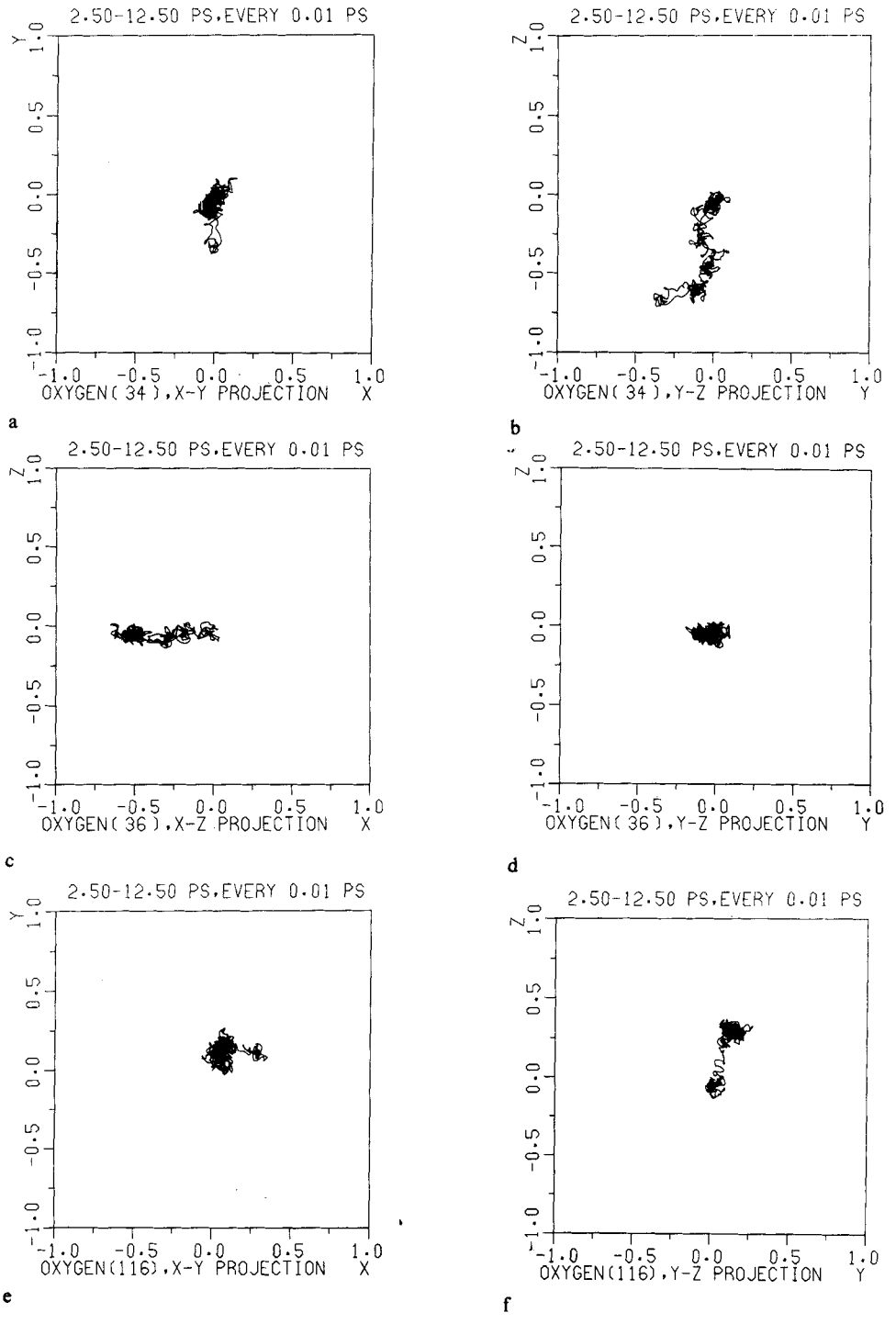

Figure 11 Selected projections of migrating O^{2-} ions. The size of each plot corresponds to the size of the simulation box.

ism of ion migration lies somewhere between a hopping mechanism and a liquid-like diffusion model. This indeed was to be expected, as it is the only mechanism compatible with a substance having simultaneously the properties of high entropy (favoring a liquid-like diffusion process) and strong local structure (favouring a hopping mechanism).

One rather significant discrepancy is that between the diffusion coefficients calculated from MSDs and VAFs. The MSD is based on a single time origin whereas the VAF involves an average over all (2 048) time origins. It therefore has much better statistics. In a system like the Bi^{3+} sub-lattice of δ-Bi_2O_3, where no jumps are observed in the time-scale of the computer experiment, the mean square displacement of Bi^{3+} ions is essentially zero and the small (sometimes negative) values of D determined by linear regression result from the oscillations in MSD caused by the vibration of the atoms. Thus a negative value can easily result from fortuitously picking $t = 0$ at a peak and the final t at a minimum. The much larger values of D that results from the VAF are caused by the contribution of velocity components that do not result in a hop between sites. In a fluid these velocity components represent a genuine contribution to D. But in a crystal (non-liquid like sub-lattices) necessary prerequisites to a successful jump are the presence of a vacant (lattice or interstitial) site to jump into, and the possession of the necessary velocity to surmount the potential barrier between sites. Even when no jumps are recorded during and MD simulation there will be many attempts in which an atom makes a much larger excursion than average from its equilibrium position. These unsuccessful attempts nevertheless contribute to the VAF and, when the jump frequency is very low, result in a higher value for the diffusion coefficient being determined from velocity correlation than from actual displacements. In a liquid-like situation, where a longer proportion of these bigger-than-average displacements become successful jumps, the difference between D calculated from MSD and D from velocity autocorrelation will be much smaller, even perhaps approaching zero in cases of limitingly high diffusion. However, in intermediate cases one should normally expect a higher value for D from the VAF than from the MSD.

Acknowledgement

This research was supported by the Natural Sciences and Engineering Research Council of Canada.

References

[1] D.A. Mac Dónaill, P.W.M. Jacobs and Z.A. Rycerz, "Molecular Dynamics Simulation of the Fast-Ion Conductor δ-Bi_2O_3", II. Sub-lattice structure", *Molecular Simulation*, **5**, 193–214 (1990).

[2] D.A. Mac Dónaill, P.W.M. Jacobs and Z.A. Rycerz, "Molecular Dynamics Simulation of the Fast-Ion Conductor δ-Bi_2O_3", *Molecular Simulation*, **3**, 155–165 (1989).

[3] L.G. Sillén, "X-Ray Studies in Bismuth Trioxide" *Arkiv Kemi Mineral. Geol.*, **12A** (18), 1–15 (1937).

[4] G. Gattow and H. Schröder, "Die Kristallstruktur der Hochtemperaturmodifikation von Wismut(III)-oxid (δ-Bi_2O_3)", *Z. anorg. allg. Chem.*, **318**, 176–189 (1962).

[5] H.A. Harwig, "On the Structure of Bismuth Sesquioxide: the α, β, γ and δ-Phase", *Z. anorg. allg. Chemie*, **444**, 151–166 (1978).

[6] M. Tsubaki and K. Koto, "Superstructures and Phase Transitions of δ-Bi_2O_3", *Mat. Res. Bull.*, **19**, 1613–1620 (1984).

[7] D.A. Mac Dónaill and P.W.M. Jacobs, "On the Lattice Parameter of some Sesquioxides with the Fluorite Structure", *J. Solid State Chem.*, **84**, in press.

[8] H.A. Harwig and A.G. Gerards, "The Polymorphism of Bismuth Sesquioxide", *Thermochim. Acta*, **28**, 121, (1979).

[9] L. Van Hove, "Correlations in Space and Time and Born Approximation Scattering in Systems of Interacting Particles", *Phys. Rev.*, **95**, 249 (1954).
[10] J. Moscinski and P.W.M. Jacobs, "Computer Simulation of Defect Motion in Model Normal and 'Fast Ion' Conductors. II. $SrCl_2$", *Proc. Roy. Soc. (Lond.)*, A, **398**, 173–201 (1985).
[11] P.W.M. Jacobs and Z.A. Rycerz, "Molecular Dynamics of α-AgI", *Cryst. Latt. Def and Amorph. Mat.*, **15**, 337–343 (1987).
[12] E.G. Pettsol'd, "Evaluation of the Density of States and Effective Mass in Bismuth Oxide", Deposited Doc., VINITI, 811–84, 12 pp. (1984) (Russian). Available from VINITI, U.S.S.R. This paper was listed in Chemical Abstracts under E.G. Petsol'd (sic.). Reference CA-102:119887f.